

# Long-term static and dynamic monitoring to failure scenarios assessment in steel truss railway bridges: A case study

B. Torres<sup>\*</sup>, P. Poveda, S. Ivorra, L. Estevan

Department of Civil Engineering, University of Alicante, P.O. Box 99, 03080 Alicante, Spain

## ARTICLE INFO

### Keywords:

Long-term monitoring  
Steel truss railway bridge  
Vertical deflection  
Modal frequency  
Failure detection

## ABSTRACT

The latest studies on failures in steel truss-type bridges found that they are highly vulnerable to damage and thus prone to potential local or total collapse. Many authors recommend monitoring the critical elements in the existing steel truss-type bridges in real time to anticipate any failures in local members. Although mechanical strain is the most frequently used variable for this purpose, this method also happens to be the most expensive monitoring strategy. This paper describes a case study of failure scenarios assessment in a steel truss-type railway bridge after extensive long-term monitoring conducted by the authors, based on measuring vertical deflections and modal frequencies. The structure has both an isostatic and a hyperstatic configuration, and was assessed by means of a combination of: (i) long-term monitoring results, and (ii) a finite element analysis to simulate several failure scenarios. A sensitivity study of the different failure scenarios has been carried out, identifying those that can be detected. The results are used to define practical recommendations for failure detection by measuring vertical deflections and modal frequencies.

## 1. Introduction

Transport infrastructures are important elements in the field of civil engineering. Measuring their structural behavior under in-service loads and environmental conditions (long-term monitoring) has undergone rapid development over the last 20 years [1]. The total investment in transport infrastructures in Eurozone countries exceeds €1,525 billion every year, of which 60% is invested in roads and 37% in railway infrastructures, according to the OECD (2020) [2]. There are several reasons for this rapid growth, in which lower hardware costs, improved monitoring sensitivity and an increased data storage capacity can be cited [1].

All the developments in long-term monitoring have largely focused on the potential benefits of *in situ* monitoring of the structural conditions, detecting failures and structural health monitoring [1,3–8]. This aspect highlights the need to establish management and maintenance procedures to extend life-cycles as much as possible and thus obtain the optimal return on investments [9]. The infrastructures also suffer from aging, so that keeping them in good structural health ensures the safety of the users and can help to avoid structural collapses, such as the one that occurred in the Viadotto Polcevera (Genoa, Italy) in 2018 [10], resulting in the death of 43 people. Other similar disasters include the Florida International University pedestrian bridge in 2018 [11], the Xijia Express Hotel in 2020 [11], in which 29 people died, or the I-35 W Mississippi River bridge, an eight-lane steel truss arch bridge that collapsed during the evening rush hour, that involved more than 100 vehicles and 13 people killed [12].

<sup>\*</sup> Corresponding author.

E-mail address: [benjamin.torres@ua.es](mailto:benjamin.torres@ua.es) (B. Torres).

To ensure this objective, civil structures should be equipped with a Structural Health Monitoring (SHM) system [13], that can detect online in real time the various types of defects, failures or damage, and monitor strain, stress, temperature, displacement, acceleration, or other variables that offer valuable information on the physical and chemical parameters related to the structural behavior. The typical SHM system includes three major components: a sensor system, a data processing system and a structural health evaluation system [14], which can be of different types according to the specific evaluation required. Choosing the right system is crucial to obtaining reliable and valid information.

A study in the US on steel truss-type railway bridges [15,16] identified more than 500 failures in a period of 11 years (1989–2000), showing that these accidents are by no means infrequent (an average of 9.7 bridges a year in the US), and that these bridges are highly vulnerable. A common feature is that a local failure sets off the progressive collapse of the entire structure or at least a great part of it [16]. While the research on progressive building collapse is quite extensive, this cannot be said for bridge structures. There is still a long way to go in the study of bridge structural behavior after a local failure and compiling practical recommendations for monitoring the bridges at present in service [16,17]. The vulnerability of steel truss-type bridges shows the importance of implementing long-term SHM systems, especially in those with a long service life, which can generate the most uncertainty. In this regard, the bibliography shows that valuable information on structural behavior can be obtained from long-term monitoring. Some examples reported in the literature include Catbas et al. 2008 [18], Yang et al. 2010 [19], Koo et al. 2013 [20] or Cross et al. 2013 [21], among others. All of these reveal the benefits of establishing long-term monitoring for better assessment of the condition of the structure.

Among all the variables that provide information on structures, vertical deflections and modal frequencies best reflect the general structural behavior [22]. Generally, the measurement of these variables implies the use of sensors connected through wiring to the monitoring systems. However, there are some scenarios such as the one presented in this paper in which vertical deflection measurements using conventional topography systems is a viable solution, and easier to implement from a technical and economic point of view. This is possible thanks to the structural configuration of the bridge as independent spans of each other, as well as their lengths, which allow the application of conventional topography with digital leveling systems. In turn, as they are simply supported spans, it is possible to identify the main vibrational behavior by using a reduced number of accelerometers. Consequently, both variables (vertical deflection and acceleration) can be measured easily, and the information obtained can be used to detect possible deviations in the behavior of the structure. It is obvious that mechanical strain, i.e., stress, provides important information for assessing structures, even though this variable refers to a stress state at a certain point in the structure. This means that local failures can only be detected by a sensor close to the initial failure point [22,23], which requires several sensors placed in the same element. Extrapolating the conclusions obtained in [22,23], a monitoring strategy based on strain sensors requires a large number of units, which tends to involve high economic, technical and labor costs, as can be seen from the actual cases [24].

In view of the vulnerability of steel truss-type bridges and the limited number of studies on failures and collapses in which they were involved [16,22,23,25–31], this paper describes a case study of a steel truss railway bridge built in 1914, in which different failure scenarios were analyzed that could be detected by long-term monitoring of vertical deflections and modal frequencies. The results of the study were obtained from long-term monitoring of vertical deflections and modal frequencies, together with their variability in time and their relationship with thermal fluctuations. Based on the results obtained, a Finite Element Model was calibrated to reproduce the different failure scenarios, and to study how they affected the structural response in terms of vertical deflections and modal frequencies. The analysis was carried out on both the isostatic and hyperstatic spans that configure the structure of the bridge. These results were then used to identify the failure scenarios that could be detected by long-term monitoring of both parameters. Finally, a series of practical recommendations are proposed for an adequate long-term SHM system for failure detection in steel truss railway bridges.

## 2. Description of the structure

The bridge under study consists of a steel structure over the Santa Ana Canyon (Benisa, Alicante, Spain) built in 1914. It is approximately 170 m long and is formed by six spans (S1-S6) with dimensions of 21.48 + 21.12 + 42.00 + 42.00 + 21.12 + 21.48 m. The 42 m long central spans (S3 and S4) have a continuous hyperstatic structural scheme and the four lateral spans (S1, S2, S5 and S6) are isostatic (Fig. 1a). The substructure is formed by two masonry abutments and five piers, composed of four build-up U-shaped steel columns at each corner, with horizontal beams and cross bracing in both directions (Fig. 1b). The piers are supported on masonry foundations.

Each deck span consists of two parallel Pratt-type trusses with upper and lower chords, diagonals and vertical members, connected to each other by transverse beams and horizontal bracings. There is no concrete slab under the railway, which is supported by transverse joists and longitudinal beams along the full length of the bridge, transferring the superstructure's loads on the main structure. The arrangement of these elements coincides at each truss vertical member joint. The cross-section of the viaduct contains a single central railway track and a pedestrian walkway on each side protected by steel railings.

The hyperstatic spans are formed by 4 m-high trusses with 3.50 m between vertical members, while the isostatic spans comprise 2.30 m-high trusses and 1.79 m between vertical members. All spans consist of 12 truss panels and the spacing between trusses is 2.80 m along the entire length of the bridge. The upper and lower chords have the same T-shaped section, the only difference being that the lower chord is inverted, i.e., the web is above the flanges. The diagonals and vertical members are formed by 4 L-shaped frames, while the joists and longitudinal beams under the railway have a double-T cross-section. The connection between the different elements of the deck and piers is made by means of plates, angles and button-headed rivets. The chords were strengthened in some areas by a set of plates and angles connected with high-strength bolts, during a series of repair works carried out in 2018. Regarding the truss supports on the piers, the hyperstatic 42 m-long spans are fixed on the central pier with a hinge support, with two roller supports at both ends.



**Fig. 1.** (a) General view of the bridge; (b) steel pier between spans S2-S3; (c) detail of isostatic span support on a short corbel; (d) train on span S4 during a load test.

The isostatic spans have one hinge and one roller support in all cases. The spans S2 and S5, adjacent to the hyperstatic spans, rest on short corbels to compensate the different height of both trusses (Fig. 1c).

The information about the bridge is complemented by Fig. 1d, which shows a train passing over span S4 during one of the scheduled load tests. On the other hand, Fig. 2 shows a general view of the viaduct, a sketch with the structural configuration of the different spans, and a cross-section detail of both isostatic and hyperstatic spans, showing the position of the accelerometers installed for the vibrational measurements. Finally, with respect to steel, the mechanical properties have been determined in previous studies [23], so only the data necessary for the analysis proposed in this paper are here specified: yielding strength, 271 MPa; ultimate strength, 399 MPa; elastic modulus, 210 GPa; and density, 78.5 kN/m<sup>3</sup>.

### 3. Structural health monitoring (SHM) system

The SHM system installed in the structure is capable of recording not only the vibrations produced by passing trains but also strain, displacement, wind and temperature. The vertical deflections caused by the trains are measured by topography techniques, based on digital leveling systems. As the topography surrounding the bridge under study made it almost impossible to monitor deflections in real time, this parameter was measured at certain times by means of a Leyca LS15 optical level [32] with a precision of 0.2 mm and a maximum horizontal range of 110 m. The deflections were recorded at the center of the six spans (S1-S6). The procedure consists of a series of time-scheduled static load tests, which involves temporarily stopping the train network for a period of approximately one and a half hours. During this interval, technicians access the structure to measure the vertical deflections. The same empty train (without passengers) is always used, so that the same load on the structure is guaranteed in all tests. This measurement method implies the handling of the equipment by two specialized technicians. One of them places the reading element on the measurement point, in this case the center of the span. The other technician installs the station in one of the abutments, an area outside the structure and non-deformable by the train. The procedure involves four phases in each span: (i) measurement of the empty structure; (ii) measurement under train load, obtaining the deflection by difference; (iii) repetition of the measure to ensure its stabilization, which in case of steel structures is practically immediate; (iv) recording of a final measurement once the load on the structure has been removed, to verify the complete recovery of the deflection without remaining values.

Vibrational behavior was measured by means of uniaxial accelerometers. Two B&K 4507-B-006 uniaxial accelerometers were placed in S1 (isostatic) and S3 (hyperstatic) spans, with a sensitivity of 490 mV/g, sufficient to avoid saturation by passing trains. The accelerometers were installed in vertical direction and at the points specified in Fig. 2. As shown, they were not installed on the longitudinal axis of the viaduct, but located on one of the lateral trusses so that the frequencies obtained were related to vertical and torsion vibrational modes. Measurements were made automatically and synchronized with the passing trains by two photocells installed before and after the bridge. The measurements lasted for 30 s, and the sampling frequency was 200 Hz. In order to satisfy the Nyquist-Shannon theorem, and to avoid problems associated with the low sampling frequency, the acquisition system was configured



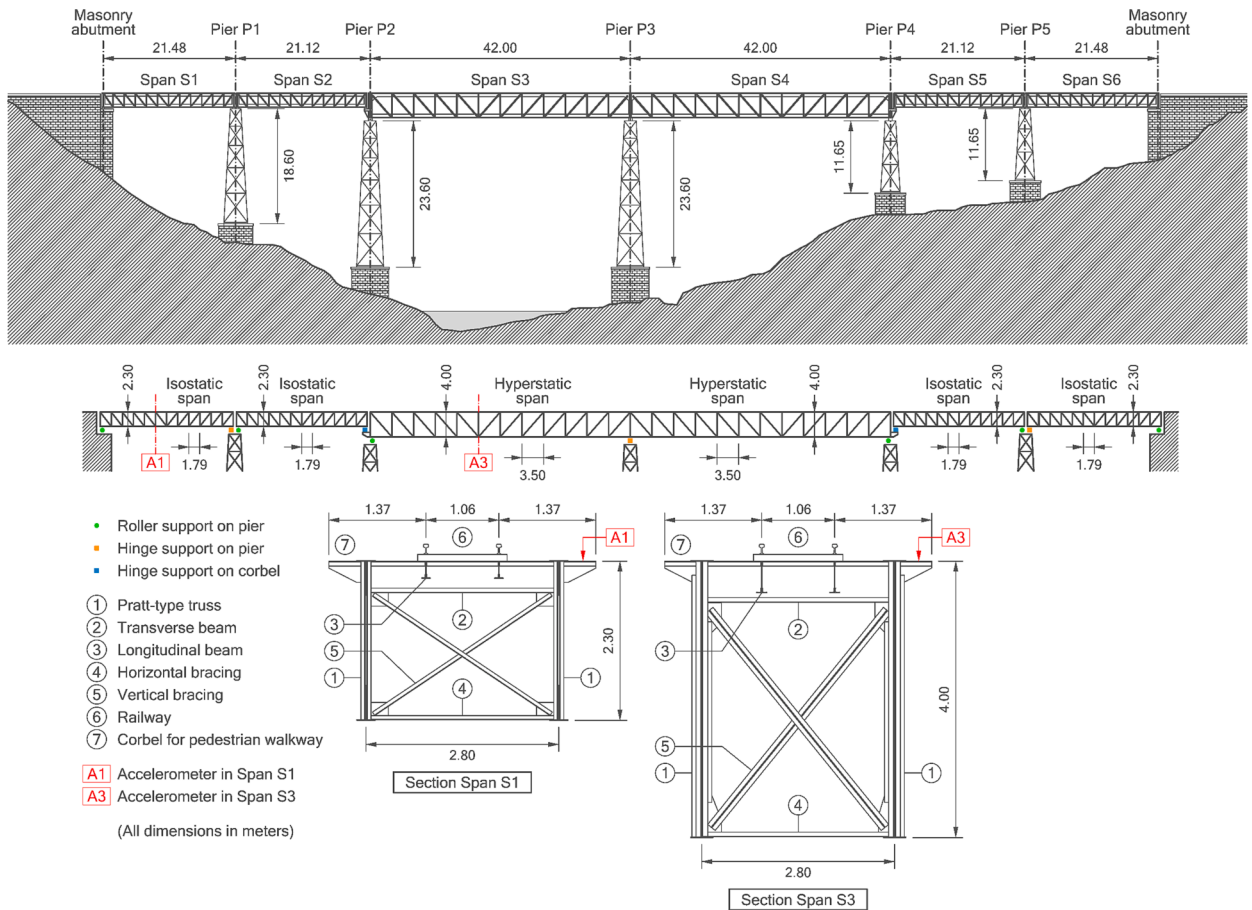


Fig. 2. General view of the viaduct, structural configuration, and cross-section detail of both isostatic (S1) and hyperstatic (S3) spans.

to include an anti-aliasing filter with a cut-off frequency of 20 Hz, a sufficient range to monitor the main modes of the structure. The signals were subsequently analyzed to obtain the vertical vibration modal frequencies of each span.

Finally, ambient temperature was also recorded by a set of thermocouples, to identify any possible thermal effects in the structural response of the bridge.

#### 4. Modal analysis of failure detection

The structural monitoring systems included not only accelerometers but also temperature, humidity, strain, vision systems and unmanned aerial vehicles, or drones, equipped with different sensors [33–36]. Among all the variables that can be measured for further analysis, SHM systems include modal analysis algorithms as their main exponent [37], so that it is essential to obtain the structure’s dynamic response. Excessive deviation from the modal frequencies, a change in its modal shapes or variations in the damping factor can be a sign of deterioration [38]. The simplest way to obtain the vibrational behavior of a structure is by installing accelerometers. In this way it is possible to determine the disturbance at a given point caused by a source of excitation. Different algorithms can be used to determine modal parameters from the information provided by the sensors.

Operational modal analysis algorithms, such as the Covariance-driven Stochastic Subspace Identification (SSI-Cov) [39], based on the State Space Model or the Frequency Domain Decomposition Method FDD [40,41], which relies on the spectral density of the vibration signal, are useful for automatic process identification [42–46]. Different metrics or indices can be found in the literature that aim to measure the level of damage produced in a structure, e.g., the modal curvature index [47], the MAC index (Modal Assurance Criterion) [48] and COMAC index (Coordinate Modal Assurance Criterion) [49]. However, the results provided by most damage indicators should be analyzed carefully since in many cases they will be affected by environmental factors or by the operating conditions of the structure. In [50–52] the influence of these factors was analyzed to diagnose damage in the Z24-bridge in Switzerland by continuous monitoring for one year. The authors established a linear correlation between the modal frequencies variations and temperature but found no relationship with humidity or wind. Another study [53] showed the relationship between modal frequency and temperature using a non-linear output-only model, which was subsequently validated on a three-span pre-stressed concrete bridge [54].



As we have seen, different tools can be used to identify possible failures in a structure by its modal behavior, although defects in real structures do not follow a regular pattern, which makes it difficult for researchers to validate the models. In this case, it is essential to use numerical tools that can simulate different structural operating conditions [55,56].

In the present study, the dynamic analysis of the structure was carried out by means of the SSI-Cov algorithm. The method starts with a pre-processing step in which the correlation matrix of the acquired signals is determined using the Welch estimator or periodogram approximation. First, the signals were divided into small blocks, considering a 50% overlap and a Hanning window. The discrete Fourier transform (Eq. (1)) and the average correlation matrix (Eq. (2)) were calculated for each of them.

$$Y_b(\omega_j) = \sum_{k=0}^{n-1} w_k y_{b,k} e^{-k\omega_j k \Delta t} \tag{1}$$

$$\widehat{S}_{yy}(\omega_j) = \frac{1}{n_b} \sum_{b=1}^{n_b} Y_b(\omega_j) Y_b(\omega_j) \tag{2}$$

The SSI-Cov method is based on the identification of the model using state variables included into the State Space Model represented in Eq. (3) and Eq. (4):

$$\dot{x}(t) = Ax(t) + Bu(t) \tag{3}$$

$$\dot{y}(t) = Cx(t) + Du(t) \tag{4}$$

where  $\dot{x}(t)$  is the state vector;  $\dot{y}(t)$  is the output vector;  $u(t)$  is the control vector;  $A$  is the state matrix;  $B$  is the input matrix;  $C$  is the output matrix; and  $D$  is the feedforward matrix.

The modal parameters may be obtained from Eq. (5), with  $\Psi$  the eigenvector matrix and  $\Lambda$  the eigenvalue matrix:

$$A = \Psi \Lambda \Psi^{-1} \tag{5}$$

Therefore, taking advantage of the relationship between the correlation matrix and the state space matrix, the behavior of the structure can be determined with Eq. (6), where  $G$  is the outputs of the next state:

$$R_j = CA^{j-1}G \tag{6}$$

To do this, first, a Toeplitz matrix must be composed and defined according to Eq. (7):

$$T_{1j_b} = \begin{bmatrix} R_{j_b} & R_{j_b-1} & \cdots & R_1 \\ R_{j_b+1} & R_{j_b} & \cdots & R_2 \\ \cdots & \cdots & \cdots & \cdots \\ R_{2j_b-1} & R_{2j_b+2} & \cdots & R_{j_b} \end{bmatrix} \tag{7}$$

Subsequently, a verification of the stability of the poles obtained for each time block was carried out. This procedure was conducted, on the one hand, by comparing the frequency of the modes, and on the other hand, by establishing the degree of similarity between modal shapes using Modal Assurance Criterion (MAC). The analysis of the signals was carried out entirely with Matlab software, using a code based on the development of [57]. The estimation algorithm was configured to analyze the signals in 2-second blocks and to identify the system with a model of order between 2 and 50. The frequencies corresponding to the first and second modes were selected as the values with minimum distance from the reference frequencies obtained from the numerical model of the structure. For the estimation of the average value of each mode, outliers were considered to be all those results whose distance with respect to the theoretical frequency exceeded 60% of the median of the distances.

### 5. Long-term monitoring results

As mentioned above, the vibration data were acquired automatically when trains passed over the bridge, while the vertical deflection results were obtained by a series of time-scheduled static load tests, which were always carried out with the same empty train to guarantee an identical load in all tests, in the same position on all the spans. The total train load of 558.4 kN was spread over 4 bogies with a total length of 34.79 m. The dynamic tests were carried out in normal operating conditions so that the structural excitation source varied according to the train involved, the number of passengers on board, the speed of the train on entering the bridge, or the hunting oscillation which excited the structure laterally, among others.

#### 5.1. Static long-term monitoring: Vertical deflections

Fig. 3 shows the evolution of the deflections at the center of the spans in the eight static load tests programmed from July 2019 until January 2023, also the evolution of temperatures in this period. As the tests were at six-monthly intervals (in January and July), the temperature reflects the seasonal cycles. The deflections at the center of the spans show relatively constant values over time, and the variations were found to be within the precision range of the monitoring equipment, i.e., within 0.2 mm under ideal operating conditions.

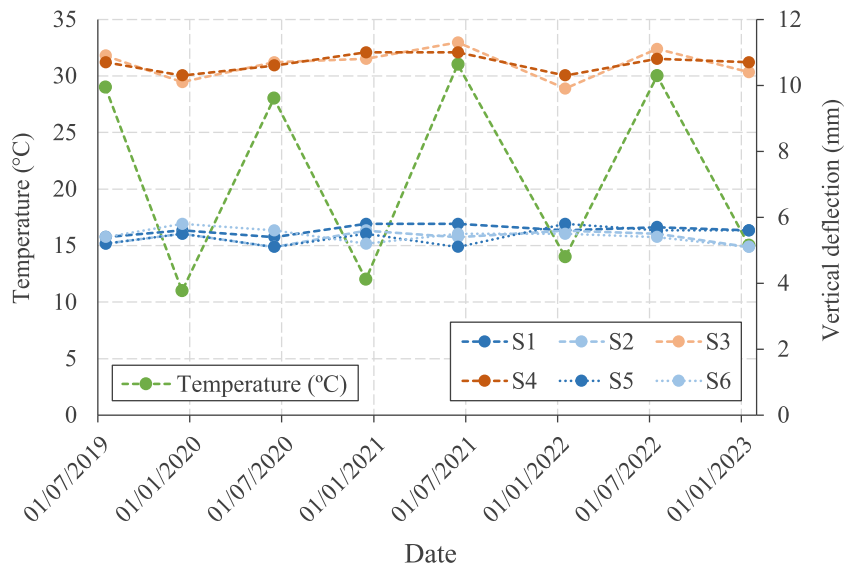


Fig. 3. Vertical deflection (mm) and temperature (°C) evolution.

Table 1

Vertical deflection average and coefficient of variation CV (%).

Span	S1	S2	S3	S4	S5	S6
Vertical deflection average (mm)	5.4	5.4	10.7	10.7	5.4	5.4
CV (%)	2.8	3.9	4.5	2.5	4.8	4.0

The mean deflection values and their associated coefficients of variation (CV) are given in Table 1. The latter were found to be quite low, due to the repeated measurements, with a maximum value of 4.8% in the S5 isostatic span. In theory, and based on the evolution of the deflections, no indications were found of a structural failure developing in the bridge that could be interpreted as compromising its safety.

However, these CV values (%) could represent the monitoring system’s minimum capacity to detect a structural failure, so that any failure or damage that varied the vertical deflections below the CV (%) would not be detected by monitoring. On the other hand, any damage that could cause the deflections to vary by more than the CV with reference to the non-failure scenario, would be identified in the vertical deflection data.

### 5.2. Dynamic long-term monitoring: Vibrations

As indicated in the previous section, the vibrational measurements were recorded automatically when a train passed over the bridge. This procedure used the trains themselves as the excitation source of the structure and shortened the time required to obtain the modal frequencies, compared to measurements based on environmental excitation. However, the method used had certain drawbacks that should be mentioned. Firstly, for the correct analysis of the vibrational behavior of the structure, it was essential to separate the components associated with the response of the bridge from those of the train, so that only the tail produced by the excitation was considered. The maximum acceleration caused by the source had to be within each signal. As acquisition was synchronized with the train entering the bridge, so that the maximum acceleration peak occurred later at the points at the opposite end of the bridge, thus reducing the useful signal for processing (see Fig. 4a, which shows two excitation signals in S1 and S3 spans during the passage of a train, offset in time). This issue increases the number of outliers, or noise, in the results obtained for the modal frequencies. Another item to be considered with respect to the method used is the characteristics of the excitation source. The length, weight and speed of the train affect the operating conditions of the structure and therefore its vibrational behavior. This could lead to an increase in the deviation margin of the modal frequencies, limiting the failure detection capacity. Fig. 4b and 4c give the maximum absolute acceleration values, similar to the Peak Ground Acceleration (PGA) occurred during an earthquake, reached in the isostatic (S1) and hyperstatic (S3) spans for the passage of the train in a period of approximately two years. These graphs show a wide variation in the vertical acceleration recorded by the sensors (bandwidth 0 – 20 Hz) since this parameter is highly dependent on the source of excitation and its characteristics. Fig. 4d shows, for illustrative purposes, a representative frequency spectrum of the measured acceleration signals.

It should be noted that various inactive periods were found in the data measurements in the months of May 2021, and September and December 2022 (Fig. 4b and 4c). The first of these was due to closure of the train network for maintenance, the second was due to a lightning strike on the structure that affected the computers and dataloggers, while the third was caused by a three-week power blackout.

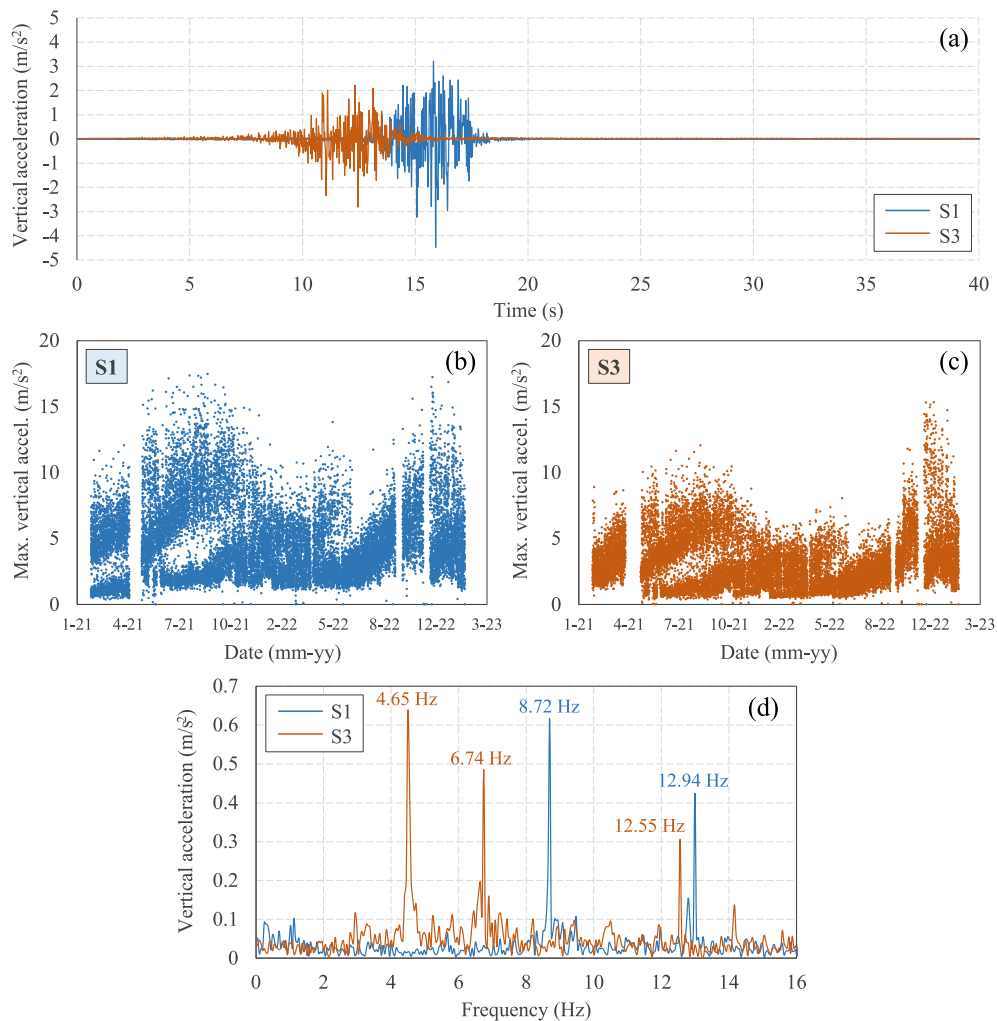


**Fig. 4.** (a) Signal measured in isostatic (S1) and hyperstatic (S3) spans; (b) and (c) maximum vertical acceleration registered in both spans; (d) frequency spectrum for both spans.

From the data obtained from the SSI-Cov algorithm, it was possible to track the modal vibrational behavior of the structure over time. Fig. 5 gives the modal frequencies associated with the vertical modes in spans S1 and S3 caused by the passing trains. The first vertical bending mode occurred at a frequency of approximately 8.9 Hz in isostatic span S1, while the mean value obtained in hyperstatic span S3 was 4.8 Hz. The second vertical modal frequency identified reached mean values of 12.8 Hz and 6.9 Hz in S1 and S3, respectively. In span S1, besides the first two frequencies recorded, a third frequency can apparently be detected around 18.6 Hz approximately, although the density of the points at this frequency level is well below the preceding ones. This means that the modal shape associated with this frequency value was rarely excited when a train passed over the bridge. Something similar happened in span S3, where in addition to the first two frequencies indicated above, a third modal form seems to be identified at around 12.5 Hz.

The other points obtained at other frequency levels referred to outliers caused by SSI-Cov algorithm identification errors. These frequency values were identified in addition to those associated with the modal frequencies and can be guaranteed not to show a drastic variation of the modal frequencies, so that their identification does not imply any uncertainty as regards possible structural failures. It should be noted however that they represent a very small percentage of the total number of the modal frequencies obtained.

The evolution of the vertical bending modal frequencies shows a significantly constant behavior. In theory they cannot be interpreted in the measured frequencies as referring to an evolving structural failure or a threat to the structural safety. In this way it is possible to determine the minimum variation that the monitoring system will be able to detect due to a structural failure. Table 2 shows the mean first and second vertical modal frequencies and their coefficients of variation CV (%) in parentheses. A failure that causes a variation in the frequencies below the CV values (%) thus cannot be identified by vibrational measurements.



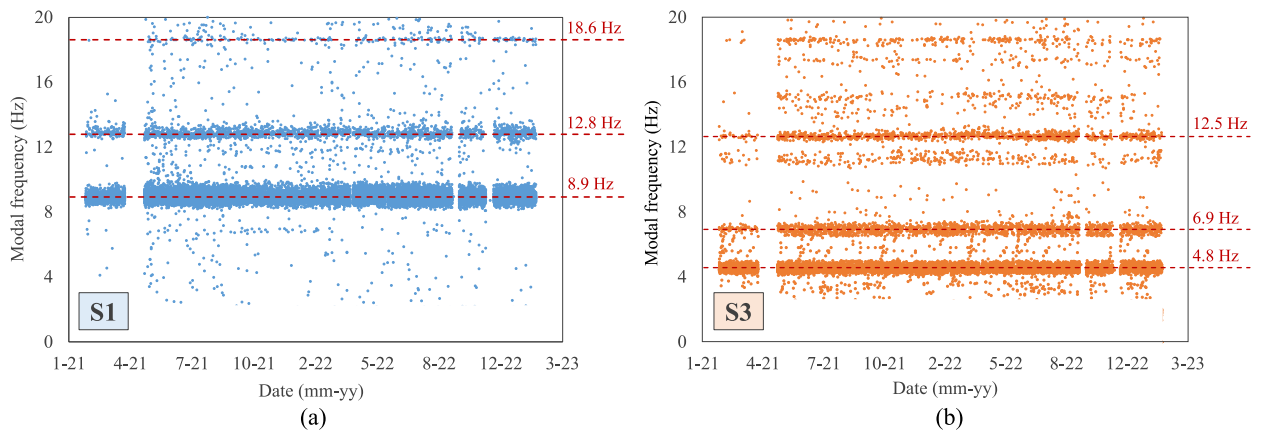


Fig. 5. Identification of modal frequencies: (a) isostatic span S1; (b) hyperstatic span S3.

Table 2

First ( $f_1$ ) and second ( $f_2$ ) modal frequencies modes for isostatic S1 and hyperstatic S3 spans. Coefficients of variation CV (%) in parentheses.

Span	$f_1$ (Hz)	$f_2$ (Hz)
Isostatic, S1	8.9 (9.1)	12.8 (6.4)
Hyperstatic, S3	4.8 (7.8)	6.9 (5.3)

### 5.3. Influence of temperature on structural response

As can be seen in Section 4, some authors [50–54] note the influence of temperature on the structural behavior by long-term monitoring systems and the importance of including environmental agents to reliably identify possible deterioration of the structure. As expected, and according to the long-term monitoring results obtained, there was no correlation between vertical deflection and modal frequencies with ambient temperature variations (Fig. 6). Temperature dependence is unexpected for steel structures without a ballast layer, especially for temperatures above freezing. In addition, the boundary conditions of the bridge allow a certain degree of free displacement, and thus dampen the variations produced by the contractions and expansions of the structure without affecting its stiffness.

## 6. Finite element modelling

After obtaining the long-term results, a Finite Element Analysis (FEA) was developed to analyze the influence of failures in the structural response in terms of vertical deflections and modal frequencies. A linear elastic FEA was implemented using SAP2000 v24 software, distributed by Computers & Structures, INC. [58]. The Finite Element Model (FEM) reproduced the bridge geometry through BEAM elements. The internal elements were fully connected (rigid joints) to each other, as this was the most appropriate assumption based on the numerical-experimental results obtained in previous studies [16,22,23]. A section designer interface was used to define

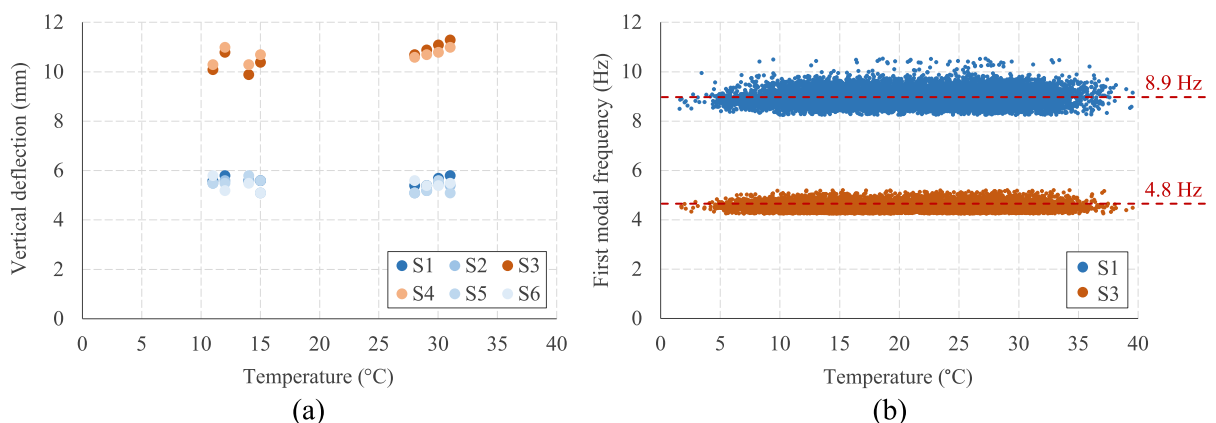


Fig. 6. Influence of ambient temperature in structural response: (a) vertical deflection (mm); (b) first vertical frequency mode in S1 and S3.

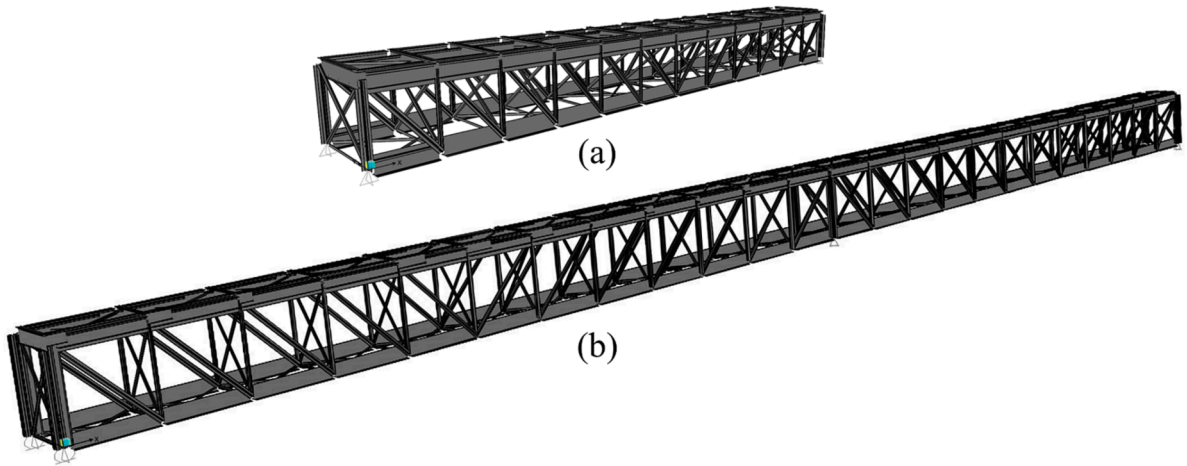


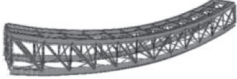





Fig. 7. FE model: (a) isostatic span S1; (b) hyperstatic span S3.

the mechanical properties of beams, including plates and angles strengthening. The steel elastic modulus was considered to be 210 GPa and the density equal to 78.5 kN/m<sup>3</sup>. The boundary conditions applied were identical to those in the structure. For the isostatic span (S1) both supports on the same side had fixed displacements and free rotation, while the two supports on the opposite side had free longitudinal displacement and rotation. In the hyperstatic span (S3), the two central supports had fixed displacements and free rotation, while the four end supports were free for longitudinal displacement and rotation. A train with identical axle spacing and weights to those used by the railway company was implemented in the FEA as point loadings. Fig. 7 shows the FE model corresponding to both spans.

6.1. Calibration of actual mechanical behavior

The model was first calibrated to reproduce the mechanical behavior of both spans. The calibration parameters were the vertical deflections at the center of the spans and the modal frequencies. The experimental results used to calibrate the models are those given in Sections 5.1 and 5.2 in this paper. The calibration in terms of modal frequencies only considered the vertical values since the uniaxial accelerometers fitted to the structure only captured vertical vibration. In the S1 span there was a first lateral bending vibration mode with a theoretical frequency of 8.8 Hz that was not considered in the model calibration and something similar happened in S3, whose first two unconsidered modal frequencies referred to lateral bending modes, with values of 3.9 and 4.0 Hz. Table 3 provides all the numerical and experimental results together with their degrees of fit. It can be seen that the numerical values reproduce the experimental results reasonably well, with similar vertical deflections and modal frequencies. Ratios range between 0.92 and 1.01 in all cases.

Table 3  
Comparison between numerical and experimental results.

		Vertical deflection, d (mm)			1 <sup>st</sup> modal frequency, f <sub>1</sub> (Hz)			2 <sup>nd</sup> modal frequency, f <sub>2</sub> (Hz)		
		d <sub>num</sub>	d <sub>exp</sub>	d <sub>exp</sub> / d <sub>num</sub>	f <sub>num</sub>	f <sub>exp</sub>	f <sub>exp</sub> / f <sub>num</sub>	f <sub>num</sub>	f <sub>exp</sub>	f <sub>exp</sub> / f <sub>num</sub>
Values	S1	5.9	5.4	0.92	9.1	8.9	0.98	14.0	12.8	0.92
	S3	11.2	10.7	0.96	4.9	4.8	0.98	6.8	6.9	1.01
Sketch	S1	 <i>Bending – single beam</i>			 <i>1<sup>st</sup> vertical bending</i>			 <i>Torsional</i>		
	S3	 <i>Bending- continuous beam</i>			 <i>1<sup>st</sup> vertical bending</i>			 <i>2<sup>nd</sup> vertical bending</i>		

6.2. Failure scenarios

Various damage scenarios were then analyzed together with their effect on the mechanical response of the structure in terms of vertical deflections and modal frequencies in order to: (i) analyze the structural robustness to damage of some elements, (ii) study the structural behavior after the activation of Alternative Load Paths (ALPs), and (iii) identify any elements in which failure had a special influence on the mechanical response of the bridge, and thus needed a damage warning. Different failure scenarios were simulated for this that included damage to the diagonals (D) at the ends of the bridge, and in the upper and lower chords (CH) at the center of the span and the support, and also considering the effect on one or both trusses. As recommended in previous studies [16,22,59,60], the damage was simulated by removing the element involved from the model, which implied assuming a local failure. Steel elements can be affected by different types of damage throughout their useful life and modelling these requires a detailed simulation of how the damage evolves and propagates, as proposed in [12,23]. However, simulating the damage by eliminating the element from the global model could also simulate a sudden break in the steel element due to fatigue cracks, an impact, an explosion, or a failure in the connecting elements between frames [16,19]. The hypothetical elimination of a damaged element is thus an effective way to evaluate the ALP activation system in a study of structural robustness to avoid a progressive collapse, an approach also used by other authors applied to both buildings and bridges.

Fig. 8 lists the elements studied in simulated failure scenarios in both the isostatic S1 and hyperstatic S3 spans, while Table 4 gives the proposed failure scenarios in which the combinations of elements indicate the failure of various members.

The above failure scenarios were quite severe in the structure under study, even though in theory they did not make it collapse. They were defined by two criteria: firstly, based on the mechanical stress results of the FEM. In case of losing a frame element (e.g., due to a fatigue crack) both structures S1 and S3 and their internal force regime distribution are seriously modified although the Von Mises stresses do not exceed the material’s maximum value, obtained from [23], i.e., 271 MPa for yielding strength and 399 MPa for ultimate strength. In this regard, Fig. 9 shows the comparative Von Mises stress distribution in the isostatic span S1 under the undamaged and 2 (CH1 + CH2) scenarios, one of the most severe hypotheses studied. This stress distribution was obtained for the most unfavorable load configuration, which corresponds with the train positioned in the center of the span. The total train load of 558.4 kN was spread over 4 bogies with a total length of 34.79 m. Each bogie has two axles, and each axle has two wheels, so the train produces a total of 16 point

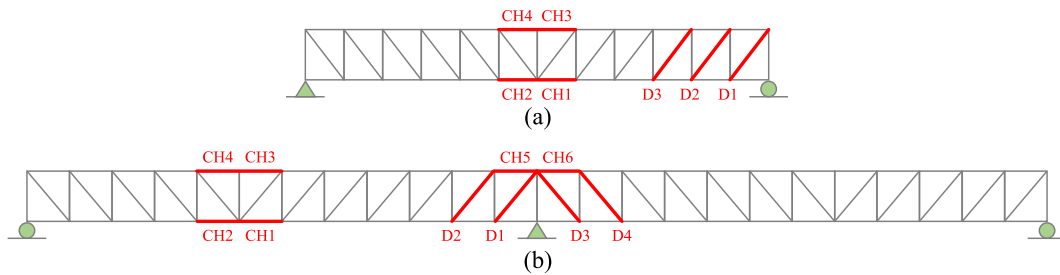


Fig. 8. Simulated damaged elements: (a) isostatic span S1; (b) hyperstatic span S3.

Table 4 Failure scenarios to be considered.

Failure scenario	Isostatic span (S1)		Hyperstatic span (S3)	
	Damaged elements	Truss	Damaged elements	Truss
Di	Diagonal i (i = 1, 2, 3)	One	Diagonal i (i = 1, 2, 3, 4)	One
2Di	Diagonal i (i = 1, 2, 3)	Both	Diagonal i (i = 1, 2, 3, 4)	Both
D1 + D2	Diagonals D1 and D2	One	Diagonals D1 and D2	One
D2 + D3	Diagonals D2 and D3	One	-	-
D1 + D3	-	-	Diagonals D1 and D3	One
2(D1 + D2)	Diagonals D1 and D2	Both	Diagonals D1 and D2	Both
2(D2 + D3)	Diagonals D2 and D3	Both	-	-
2(D1 + D3)	-	-	Diagonals D1 and D3	Both
D1 + D2 + D3	Diagonals D1, D2 and D3	One	-	-
2(D1 + D2 + D3)	Diagonals D1, D2 and D3	Both	-	-
CHi	Chord i (i = 1, 3)	One	Chord i (i = 1, 2, 3, 4, 5)	One
2CHi	Chord i (i = 1, 3)	Both	Chord i (i = 1, 2, 3, 4, 5)	Both
CH1 + CH2	Chords CH1 and CH2	One	Chords CH1 and CH2	One
2(CH1 + CH2)	Chords CH1 and CH2	Both	Chords CH1 and CH2	Both
CH3 + CH4	Chords CH3 and CH4	One	-	-
2(CH3 + CH4)	Chords CH3 and CH4	Both	-	-
CH1 + CH3	Chords CH1 and CH3	One	Chords CH1 and CH3	One
2(CH1 + CH3)	Chords CH1 and CH3	Both	Chords CH1 and CH3	Both
CH5 + CH6	-	-	Chords CH5 and CH6	One
2(CH5 + CH6)	-	-	Chords CH5 and CH6	Both



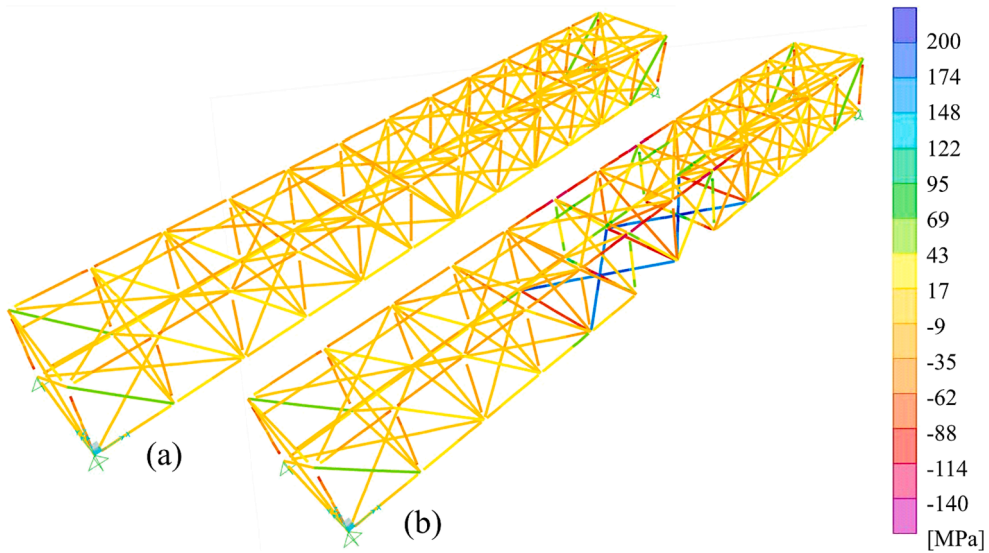


Fig. 9. Von Mises stress distribution strongly modified in isostatic span S1: (a) undamaged; (b) 2(CH1 + CH2) failure scenario.

loads. Since the total length of the train is greater than the total span length, only the two center bogies, which represent 8 point loads of 31.45 kN, are applied on the structure. It should also be noted that the stress distribution indicated corresponds to the self-weight of the structure plus the train loads, without any factor of safety.

Fig. 9 shows the activation of the ALPs in which the lower horizontal bracing plays a fundamental role in redistributing the stresses: while the maximum stress in the undamaged scenario is 45 MPa, values of up to 223 MPa in the lower crosses after the failure are reached. However, although the stress is elevated, it can be seen that the values are far from the steel yielding strength. Secondly, the failure scenarios were then defined by the results of previous studies [16,22], in which full-scale experimental robustness tests with numerical computer simulations (that did not involve a structural collapse) were carried out on a type of bridge with similar characteristics to the one analyzed in the present study.

### 6.3. Vertical deflections

Fig. 10 shows the deformed shape in both spans under the undamaged and two possible failure scenarios (affecting one or two trusses). The load configuration is the same as the one described in the previous section for the isostatic S1 span, while in S3 the full load of the train positioned in the center of the span is applied (see Fig. 1d). The behavior of both spans can be seen to differ according

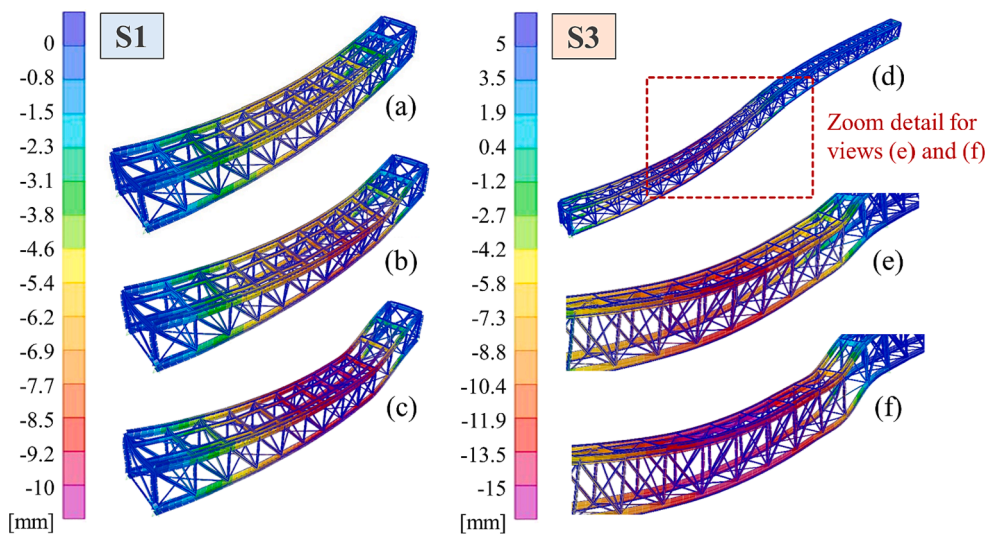


Fig. 10. Vertical deflections (mm): (a) S1, undamaged; (b) S1, failure D2 + D3; (c) S1, failure 2(D2 + D3); (d) S3, undamaged; (e) S3, failure D2; (f) S3, failure 2D2.

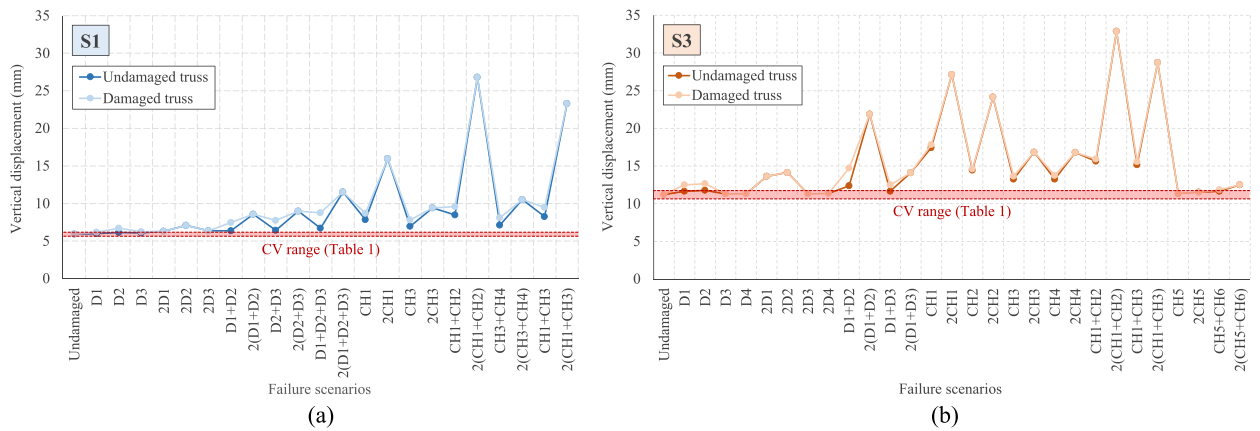


Fig. 11. Vertical deflection in different failure scenarios: (a) isostatic span S1; (b) hyperstatic span S3.

to the location of the failure. When it affects a single truss, the vertical displacements are considerably greater in the involved truss, which is asymmetrically deformed in relation to the longitudinal axis, submitting the structure to torsional effect (see Fig. 10b and 10e, the latter showing a zoom of the area where greater vertical deflections are obtained in span S3 during D2 failure scenario). On the other hand, when the failure affects both trusses, the behavior is symmetrical, as could be expected (see Fig. 10c and 10f, the latter showing a zoom of the area where greater vertical deflections are obtained in span S3 during 2D2 failure scenario). This effect seems to be more noticeable in the isostatic span S1, while in hyperstatic span S3 both trusses appear to respond more uniformly, regardless of where the damage occurs and probably due to their higher degree of redundancy.

Taking into account the above comments, Fig. 11 shows the evolution of the vertical deflections in the mid spans for the failure scenarios given in Table 4, when they occur in both undamaged and damaged trusses. When the failure is symmetrical in the two trusses the deflection is identical in both, but when only one truss is damaged, measuring the deflection in the undamaged truss, the situation is less favorable for the failure detection. Several horizontal lines are also represented in the graphs, which correspond with the upper and lower limits with respect to the deflection in the undamaged scenario –determined by the coefficient of variation CV given in Table 1– by which failure can be detected. In the isostatic S1 span, the selected CV is the least favorable of the four spans studied, corresponding to a value of 4.8%, while the CV used for the hyperstatic S3 span is 4.5%.

In view of the results, it can be seen that there are a series of failure scenarios that cannot be detected by the deflection measurements. In isostatic S1 span (Fig. 11a) the failure of any diagonal modifies the deflections below the defined by the CV of 4.8%, revealing the high robustness of the bridge structure. The D2 failure scenario could be detected exceptionally if the deflections are recorded in the damaged truss, although the D1, D2, D3 and D4 failure scenarios are unlikely to be identified from the deflection measurements. It is even unlikely to identify the failure of two or three diagonals together (failure scenarios D1 + D2, D2 + D3 and D1 + D2 + D3). In this case the variability of the deflections is very close to the upper limit imposed by the CV, so that detection is by no means certain. Again, it would be exceptional to detect these scenarios if the deflection readings are taken in the damaged truss. When the failure of two or three diagonals affects both trusses (failure scenarios 2D2, 2(D1 + D2), 2(D2 + D3) and 2(D1 + D2 + D3)) the deflections significantly exceed the upper limit defined by the CV, which guarantees an easy detection.

The variations in the vertical deflections are more sensitive to the failure scenarios in the chords at the center of the span, although it is easier to detect abnormal behavior when the failure occurs in the lower chords (CH1 and CH2). In this case, when the failure of a chord at the center of the span occurs in a single truss it can be detected (the CH1 failure scenario increases the vertical deflections by 33% with reference to the undamaged scenario and the CH1 + CH2 scenario raises it by 43% if the deflections are measured in the undamaged truss). However, it would be easier to identify if the damage occurs in both trusses since the variations in the deflection are much greater (2CH1 raises the vertical deflections by 270% with respect to the undamaged scenario). On the other hand, the structural behavior as regards deflections is less affected when the damage is in the upper chord (CH3 and CH4), since the CH3 scenario raises the vertical deflections by 17% with respect to the undamaged scenario, while CH3 + CH4 raises them by 20%. This occurs because the upper horizontal structure is more robust (bracings, beams and stringers) than the lower (bracings only) and better able to efficiently distribute the load between the nearby elements. It is, therefore, a less critical scenario as regards structural safety, but in which it is more difficult to detect this failure scenario.

Something similar happens in hyperstatic S3 span (Fig. 11b), in which the damaged lateral diagonals around the central support (D1, D2, D3 and D4) have hardly any influence in the deflection at the center of the span, that is difficult to detect by conventional topographical systems, unless the deflections are measured in the failed truss (scenarios D1 and D2 increase the deflection by 11% and 13%, respectively, with reference to the undamaged scenario, if the deflection is measured in the damaged truss). However, when the failure in the diagonals affects both trusses (scenarios 2D1) the response in terms of deflection depends on the type of diagonal considered. When the damaged diagonals are in the span in which the deflection is measured (in 2D1 and 2D2 the vertical deflections are increased by 21% and 26% with respect to the undamaged scenario) the effect is obvious and easily detectable. However, scenarios with failed diagonals in the span adjacent to the monitored one (2D3 and 2D4) are unlikely to be detected. In turn, the simultaneous

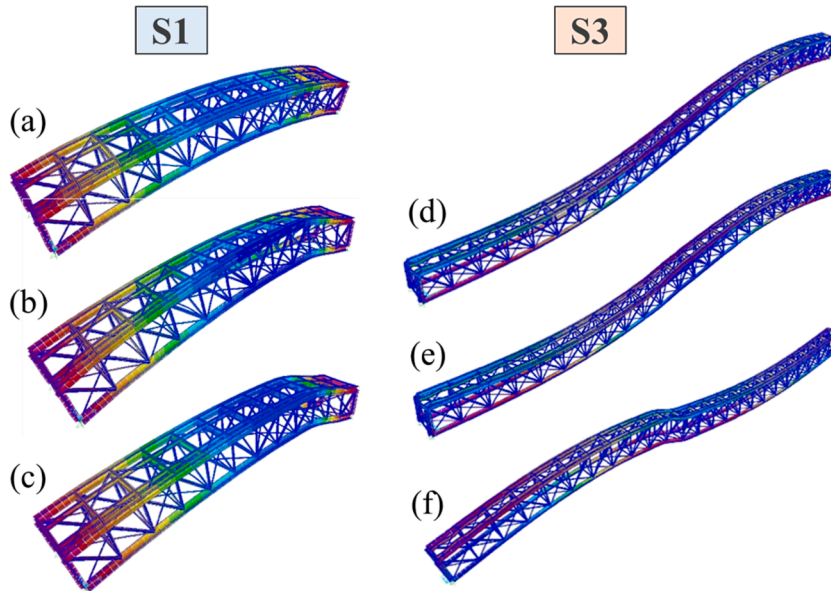


**Fig. 12.** Modal deformed shape: (a) S1, undamaged; (b) S1, failure D2 + D3; (c) S1, failure 2(D2 + D3); (d) S3, undamaged; (e) S3, failure D2; (f) S3, failure 2D2.

failure of two diagonals can be identified as long as both trusses are affected (scenarios 2(D1 + D2) and 2(D1 + D3)). If only one truss is damaged (D1 + D2 and D1 + D3), detection is assured if the deflection is monitored in the damaged truss. On the other hand, as happened in isostatic S1 span, the variation of the deflection is more sensitive in the scenarios in which the failure occurs in the chords at the center of the span, although it is true that the failure in the upper chord has a smaller effect on the deflection since the upper horizontal structure is more robust than the lower. Failure scenarios were also evaluated in upper chords in the central support system (scenarios CH5 and CH6); when these elements fail there is practically no effect on the deflection, which means it is impossible to detect.

#### 6.4. Modal frequencies

Fig. 12 gives the modal deformed shape in both spans in the undamaged and under two of the simulated failure scenarios (damage in one or two trusses in each case). The behavior of both trusses differs according to the location of the failure, with an asymmetric modal frequency with reference to the longitudinal axis when the failure is in one truss only (Fig. 12b and 12e). This effect is clearly more perceptible in the isostatic S1 span, while in hyperstatic S3 span both trusses appear to respond more uniformly. When both trusses are affected, the failure is symmetrical (Fig. 12c and 12f), as could be expected. The effect of failure can modify the modal deformed shape, especially in the case of 2D2 in hyperstatic span S3, in which the first modal deformed shape changes radically with respect to the undamaged scenario (Fig. 12f).

Fig. 13 shows the evolution of the first two vertical modal frequencies for the different failure scenarios studied. A set of horizontal lines are also shown that, similarly to the deflection analysis, represent the upper and lower limits of the frequencies –determined from the CV (%) shown in Table 2– used to failure detection. In isostatic S1 span, the CV selected for the first modal frequency is 9.1% and 6.4% for the second. For hyperstatic S3 span, the CV used is 7.8% for the first and 5.3% for the second modal frequency. In general, it can be seen that the S3 results (Fig. 13b) vary less than those for S1 span (Fig. 13a) under the different failure scenarios simulated, so that it appears to be more difficult to detect a failure in S3 from the vibrational measurements. This is due to its greater structural redundancy, which in the event of a possible failure activates ALP mechanisms more effectively, so that many of the scenarios cannot be detected in S3 from the frequency register data.

In hyperstatic S3 span (Fig. 13b), failure of the diagonals does not cause the first modal frequency to vary significantly, except when the failure occurs in two diagonals of both trusses (scenario 2(D1 + D2) reduces the first modal frequency by 18% with respect to the first modal frequency in the undamaged scenario). However, this type of failure has a greater effect on the evolution of the second modal frequency, which undergoes considerable variations in scenarios with damage in both trusses (2D1, 2D2, 2D3, 2D4, D1 + D2, 2(D1 + D2), D1 + D3 and 2(D1 + D3)). A failure in a single truss diagonal causes variations close to the lower CV limit (scenarios D1, D2, D3 and D4 reduce the second modal frequency by approximately 5%), which implies uncertainty in detecting these failure scenarios. On the other hand, a failure in central-span chords would cause detectable variations in the first modal frequency but undetectable in the second (scenario CH1 reduces by 9% the first modal frequency with reference to the undamaged scenario and 2CH1 reduces it by 20%), while damage in the upper chord (CH3 and CH4) could not be identified from the frequency readings due to its greater degree of structural redundancy. Finally, failure of the upper chords on the central support are scarcely perceptible in the response in terms of



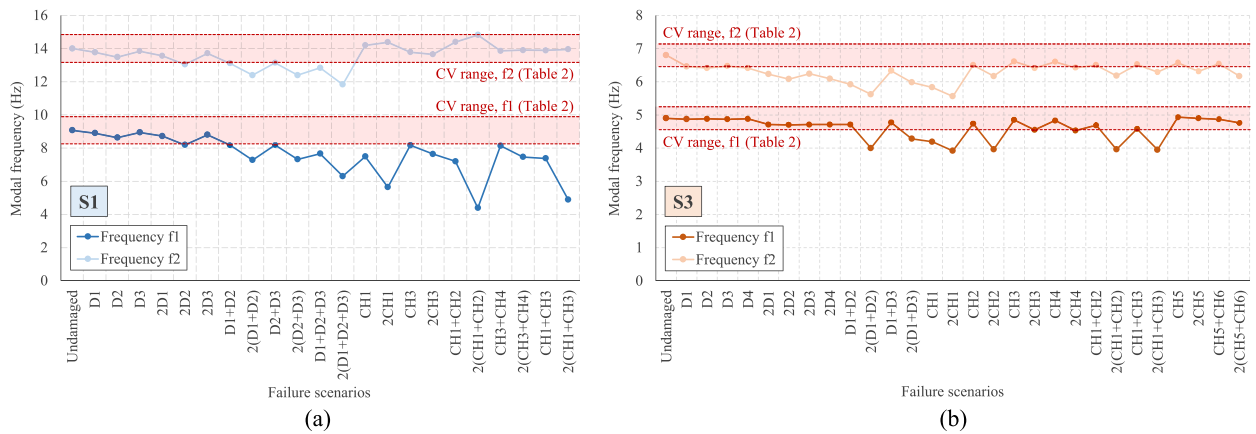


Fig. 13. Frequency (Hz) evolution in different failure scenarios: (a) isostatic span S1; (b) hyperstatic span S3.

modal frequencies in either one or two trusses (scenarios CH5, 2CH5, CH5 + CH6 and 2(CH5 + CH6)).

In isostatic S1 span (Fig. 13a), the first modal frequency is more sensitive to variations caused by the studied failure scenarios, while the second modal frequency has smaller variations, which are therefore more difficult to use for detecting failure scenarios. As in hyperstatic S3 span, failures in the diagonals appear to be in general difficult to detect from the frequency readings. In exceptional circumstances a failure would be detectable in two or three diagonals in both trusses (2(D1 + D2), 2(D2 + D3) and 2(D1 + D2 + D3)). On the other hand, failures in the lower chords in the central span could be detected, even in a single truss (scenario CH1 reduces the first modal frequency by 18%), but failure in the upper chords causes variations in the modal frequency very close to the lower limit, which would make detection difficult. These variations are significantly amplified with failures in both trusses. As regards the second modal frequency, as previously indicated, its variation is small in any failure scenario, so that detection of a failure is unlikely by this variable. Detection by the second modal frequency is only possible with severe damage in both trusses and involving several diagonals.

### 7. Discussion of vertical deflection and modal frequency measurements for failure detection

Most authors of analytical studies of bridge robustness recommend monitoring critical elements in real time, especially in cases that do not comply with the robust criteria, to anticipate the complete failure of a local element that could cause a progressive collapse [16,22]. The analysis can be carried out by means of strain, displacement, or acceleration sensors. As indicated in Section 1, monitoring strategies based on strain sensors require a large number of units, a strategy that is costly in technical and financial terms and workload. Vertical deflection and modal frequencies provide information on the general behavior of a structure, can be obtained from relatively few measurement points and are cheaper and simple to carry out, compared to other monitoring systems such as based on strain sensors. This section discusses some of the recommendations for long-term and real-time monitoring of steel truss-type bridges for failure detection, based exclusively on measurements of vertical deflections and modal frequencies.

In view of the results obtained from the theoretical analysis by the FEM, the two structures studied (S1 and S3 spans) have shown their capacity to adapt to a failure in key elements such as diagonals and the upper and lower longitudinal chords, thanks to the redundancy built into this type of structure. Structural continuity is also especially important in the joints to give the structure sufficient ability to absorb bending stresses. This last recommendation is not common when designing Pratt-type trusses, but should be addressed if the aim is to achieve a robust structure. This concept means that the structure can activate ALPs to avoid a collapse. The numerical analysis shows the activation of the previously described ALPs in each of the simulated failure scenarios.

The failure of certain elements has an almost negligible effect on the overall behavior of the structure as regards deflections and modal frequencies. This is the case, for example, with the diagonals in both the isostatic S1 and hyperstatic S3 configurations. Thanks to their structural redundancy, both structures can adapt to the failure of a diagonal not only without collapsing, but also making it difficult to detect, unless the deflection measurements were taken in the actual damaged truss. However, when the damage is in the chords at the center of the span, its effect on the structural response depends on its exact position, so that in both S1 and S3 spans any damage in the lower chord has a greater effect than if it occurs in the upper chord. Damage to the lower chord can be detected with certainty, but there would be serious doubts on the correct detection of failure to the upper chord.

In both isostatic and hyperstatic configurations, deflection is generally the most variable factor in a failure scenario and also provides the most valuable information for the detection of the greatest number of failure scenarios. As can be deduced from the types of deformed shapes in different failure scenarios (Fig. 10), detection can be improved by registering multiple points in both trusses, besides the deflections at the center of the span. As can be seen in Fig. 14, which shows the deflections (measured in damaged truss) corresponding to the undamaged, D2 and 2D2 scenarios for S1 and S3 spans, damage can be localized more precisely using this strategy. It can be clearly observed that the deflection measurements at multiple points helps to identify and locate failures earlier. In this case, in S1 span, the damage simulated in diagonal D2 causes a greater distortion in deformed shape between 3.58 and 5.37 m (Fig. 14a). Something similar happens in S3 span, in which the failure in D2 produces a marked distortion in deflections between 35 and 38.5 m (Fig. 14b).

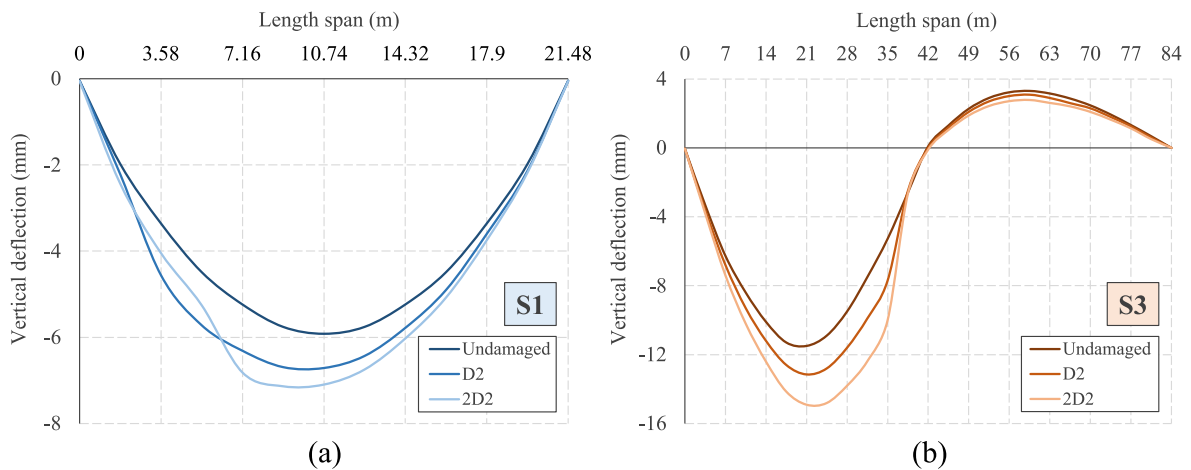


Fig. 14. Vertical deflection along the span in undamaged configuration, D2 and 2D2 failure scenarios: (a) isostatic span S1; (b) hyperstatic span S3.

As regards the failure analysis, the modal frequency is a variable that is generally less affected than deflection in a failure scenario, with larger variations in the first than the second frequency. Hyperstatic S3 span presents better robustness than S1, since its modal frequencies vary less in a failure scenario such as those studied in the present paper. The same does not happen in the isostatic S1 span, whose first modal frequency presents variations that are able to detect under certain hypotheses of damage. This is basically due to two aspects: the first is the already commented structural redundancy of the hyperstatic S3 span, with its better capacity to generate ALPs. The second is the variability of the data registration. The modal frequency presents a greater variability than the vertical deflection since it mostly depends on the source of the excitation (the weight of the train, the speed, hunting oscillation, etc.). These factors give greater dispersion to the dynamic response of the structure and make it difficult to detect the failure, based on this parameter. Throughout the study, the acceleration sensors and FFTs showed that the modal frequencies of the structure were significantly reduced only in the case of severe and multiple damage, practically when the failure occurs simultaneously in the elements in both trusses. The exceptions in this case are those in the lower chord at the center of the span, which can be detected by the vibrational measurements.

By using a uniaxial accelerometer at the mid span, it would be possible to precisely identify the modal frequencies corresponding to vertical bending and torsion in isostatic S1 span, and the vertical bending as a continuous beam in hyperstatic S3 span. However, using more accelerometers to capture more vibrational modes does not appear to be a good solution for the detection of failure scenarios in this type of structure, since there are few variations in its second modal frequency. In fact, vibration-based methods of structural failure detection are typically based on monitoring changes of parameters more sensitive than frequency, such as the mode-shape curvature or the curvature of the Frequency Response Function [16,61]. For these reasons, although it is somewhat difficult to anticipate any local failure by monitoring the modal frequencies, it is not impossible.

Bearing in mind all the above considerations, Table 5 gives in different colors the failure scenarios that can be detected with certainty (in green), with a degree of uncertainty (orange) and those that cannot be detected (red), by registering the vertical deflections and the modal frequencies. Since the importance of registering not only the deflections at the center of the span but also at other points in the structure in both trusses has already been pointed out, in Table 5 the deflections registered in the damaged truss were also considered as well as the first vertical modal frequency. As regards the qualitative aspect, and emphasizing the comments given above, Table 5 shows that it is easier to detect a failure in isostatic S1 span than in hyperstatic S3 span. In the same structure, deflection is the variable that provides the most information for failure detection.




## 8. Conclusions

This paper describes a case study of failure scenarios assessment in a steel truss-type railway bridge built in 1914 in Alicante (Spain), which has been subjected to extensive long-term monitoring by the authors for several years, analyzing a large data archive of vertical deflections and modal frequencies. Although mechanical strain is a key variable in identifying the real structural behavior, it involves expensive monitoring strategies. The present study consisted of: (i) the long-term monitoring results, and (ii) a Finite Element Analysis (FEA) to simulate several failure scenarios. The objective was to identify the local failures that can be detected by measuring the vertical deflections and modal frequencies, to show the suitability of both variables for failure detection. After the analysis, some conclusions and recommendations can be made:

- The long-term vertical deflection and modal frequency monitoring results do not indicate that the structure under study is likely to present a failure serious enough to threaten its safety. The evolution of both parameters showed a constant tendency, regardless of the thermal variations experienced by the structure over time.
- Although the failure scenarios simulated in the structure were quite severe, many of them could not be detected from the measured vertical deflections or modal frequencies. Thanks to their structural redundancy, both the isostatic and hyperstatic spans were able

**Table 5**  
Failure scenarios in both structures and possibility of detection in each case.

Failure scenario	Isostatic span (S1)		Hyperstatic span (S3)	
	Vertical deflection	Modal frequency	Vertical deflection	Modal frequency
D1				
D2				
D3				
D4	-	-		
2D1				
2D2				
2D3				
2D4	-	-		
D1 + D2				
D2 + D3			-	-
D1 + D3	-	-		
2(D1 + D2)				
2(D2 + D3)			-	-
2(D1 + D3)	-	-		
D1 + D2 + D3			-	-
2(D1 + D2 + D3)			-	-
CH1				
CH2	-	-		
CH3				
CH4	-	-		
CH5	-	-		
2CH1				
2CH2	-	-		
2CH3				
2CH4	-	-		
2CH5	-	-		
CH1 + CH2				
2(CH1 + CH2)				
CH3 + CH4			-	-
2(CH3 + CH4)			-	-
CH1 + CH3				
2(CH1 + CH3)				
CH5 + CH6	-	-		
2(CH5 + CH6)	-	-		

Color code:  Failure scenarios that could be reliably detected  
 Failure scenarios detectable with uncertainty  
 Non-detectable failure scenarios

to adapt to the failure and not only avoid collapse, but also show that the detection is unlikely by the deflections or modal frequencies measured at the center of the span.

- In general, a failure in any diagonal is difficult to detect by monitoring deflections and modal frequencies, while those in the upper chord have less effect than failures in the lower chord. This occurs since the upper horizontal structure is more robust (with bracings, beams and stringers) than the lower (with bracings only) and more efficiently able to distribute the load between nearby elements.
- In both isostatic and hyperstatic configurations, deflection is the variable that changes most in a failure scenario, and the one that provides the most valuable information for the detection of potential damages. Failure detection may be more successful by registering not only the deflections at the center of the span, but also at other points in both trusses, which would provide information of the precise location of the damage.



- The modal frequency is generally less affected than the deflection in a failure scenario, as the first frequency goes through larger variations than the second. A single vertical uni-axial accelerometer at the center of the span installed laterally in one of the two trusses can identify with precision the frequencies of the modal shapes associated with the vertical or torsional modes. Using more accelerometers to capture more vibration modes does not appear to be a good method of failure detection in this type of structure, since very few variations can be detected by the second modal frequency.
- The long-term monitoring of vertical deflections and modal frequencies involves the use of a small number of sensors and relatively few measuring points, which implies a cheaper and easier strategy compared to other monitoring systems, such as based on strain sensors. On the other hand, continuous monitoring over time is recommended for the detection of local failures that could lead to a possible partial or total collapse of the structure, although it is important to note that some failure scenarios may not be properly identified.

### Declaration of Competing Interest

The authors declare that they have no known competing financial interests or personal relationships that could have appeared to influence the work reported in this paper.

### Data availability

Data will be made available on request.

### Acknowledgements

The authors would like to express their gratitude to FGV (Ferrocarrils de la Generalitat Valenciana), FCC Construcción S.A., CHM Obras e Infraestructuras S.A., Contratas y Ventas S.A. and CALSENS S.L., for their invaluable cooperation and recommendations.

### References

- [1] Z. Wynne, T. Stratford, T.P.S. Reynolds, Perceptions of long-term monitoring for civil and structural engineering, *Structures* 41 (2022) 1616–1623, <https://doi.org/10.1016/j.istruc.2022.05.090>.
- [2] OECD Data, Infrastructure investment. <https://data.oecd.org/transport/infrastructure-investment.htm> (accessed on October 2022).
- [3] M. Sun, W.J. Staszewski, R.N. Swamy, Smart sensing technologies for structural health monitoring of civil engineering structures, *Adv. Civ. Eng.* (2010), 724962, <https://doi.org/10.1155/2010/724962>.
- [4] S. Das, P. Saha, A review of some advanced sensors used for health diagnosis of civil engineering structures, *Meas. J. Int. Meas. Confed.* 129 (2018) 68–90, <https://doi.org/10.1016/j.measurement.2018.07.008>.
- [5] S. Sony, S. Laventure, A. Sadhu, A literature review of next-generation smart sensing technology in structural health monitoring, *J. Struct. Control Health Monit.* 26 (3) (2019) e2321.
- [6] J. Etxaniz, G. Aranguren, J.M. Gil-García, J. Sánchez, G. Vivas, J. González, Ultrasound-based structural health monitoring methodology employing active and passive techniques, *Eng. Fail. Anal.* 146 (2023), 107077, <https://doi.org/10.1016/j.engfailanal.2023.107077>.
- [7] S. Mishra, P. Sharan, K. Saara, Real time implementation of fiber Bragg grating sensor in monitoring flat wheel detection for railways, *Eng. Fail. Anal.* 138 (2022), 107077, <https://doi.org/10.1016/j.engfailanal.2022.106376>.
- [8] M. Du, X. Wang, Y. Zhang, L. Li, P. Zhang, In-situ monitoring and analysis of tunnel floor heave process, *Eng. Fail. Anal.* 109 (2020), 104323, <https://doi.org/10.1016/j.engfailanal.2019.104323>.
- [9] A. Pipinato, P. Collin, R. Hallmark, Prolonging the Lifetime of Old Steel and Steel-Concrete Bridges: Assessment Procedures and Retrofitting Interventions, *Struct. Eng. Int. J. Int.* 29 (4) (2019) 507–518, <https://doi.org/10.1080/10168664.2019.1660602>.
- [10] S. Invernizzi, F. Montagnoli, A. Carpinteri, Fatigue assessment of the collapsed XX<sup>th</sup> century cable-stayed Polcevera Bridge in Genoa, *Proc. Struc. Inte.* 18 (2019) 237–244, <https://doi.org/10.1016/j.prostr.2019.08.159>.
- [11] M. Mishra, P.B. Lourenço, G.V. Ramana, Structural health monitoring of civil engineering structures by using the internet of things: A review, *J. Build. Eng.* 48 (2022), 103954, <https://doi.org/10.1016/j.jobe.2021.103954>.
- [12] CNR-DT 214/2018, Guide to design of structures for robustness, National Research Council of Italy, Advisory Committee on Technical Recommendations for Construction, Roma (2021).
- [13] F.K. Chang, Structural Health Monitoring: A Summary Report on the First Stanford Workshop on Structural Health Monitoring, Proceedings of the International Workshop on Structural Health Monitoring, Stanford University, Sept. 18–20 (1997).
- [14] B. Torres, I. Payá-Zaforteza, P.A. Calderón, J.M. Adam, Analysis of the strain transfer in a new FBG sensor for Structural Health Monitoring, *Eng. Struct.* 33 (2) (2011) 539–548, <https://doi.org/10.1016/j.engstruct.2010.11.012>.
- [15] K. Wardhana, F.C. Hadipriono, Analysis of recent bridge failures in the United States, *J. Perform. Constr. Facil.* 17 (3) (2003) 144–150, [https://doi.org/10.1061/\(ASCE\)0887-3828\(2003\)17:3\(144\)](https://doi.org/10.1061/(ASCE)0887-3828(2003)17:3(144)).
- [16] G. Caredda, M.C. Porcu, M. Buitrago, E. Bertolesi, J.M. Adam, Analysing local failure scenarios to assess the robustness of steel truss-type bridges, *Eng. Struct.* 262 (2022), 114341, <https://doi.org/10.1016/j.engstruct.2022.114341>.
- [17] V. Sangiorgio, A. Nettis, G. Uva, F. Pellegrino, H. Varum, J.M. Adam, Analytical fault tree and diagnostic aids for the preservation of historical steel truss bridges, *Eng. Fail. Anal.* 133 (2022), 105996, <https://doi.org/10.1016/j.engfailanal.2021.105996>.
- [18] F.N. Carbas, M. Susoy, D.M. Frangopol, Structural health monitoring and reliability estimation: long span truss bridge application with environmental monitoring data, *Eng. Struct.* 30 (9) (2008) 2347–2359, <https://doi.org/10.1016/j.engstruct.2008.01.013>.
- [19] D. Yang, D. Youliang, L. Aiqun, Structural condition assessment of long-span suspension bridges using long-term monitoring data, *Earthqu. Eng. Eng. Vib.* 9 (1) (2010) 123–131, <https://doi.org/10.1007/s11803-010-9024-5>.
- [20] K.Y. Koo, J.M.W. Brownjohn, D.I. List, R. Cole, Structural health monitoring of the Tamar suspension bridge, *J. Struct. Control Health Monit.* 20 (4) (2013) 609–625, <https://doi.org/10.1002/stc.1481>.
- [21] E.J. Cross, K.Y. Koo, J.M.W. Brownjohn, K. Worden, Long-term monitoring and data analysis of the Tamar Bridge, *Mech. Syst. Signal Process* 35 (1–2) (2013) 16–34, <https://doi.org/10.1016/j.ymsp.2012.08.026>.
- [22] M. Buitrago, E. Bertolesi, P.A. Calderón, J.M. Adam, Robustness of steel truss bridges: Laboratory testing of a full-scale 21-metre bridge span, *Structures* 29 (2021) 691–700, <https://doi.org/10.1016/j.istruc.2020.12.005>.

- [23] E. Bertolesi, M. Buitrago, J.M. Adam, P.A. Calderón, Fatigue assessment of steel riveted railway bridges: Full-scale tests and analytical approach, *J. Constr. Steel Res.* 182 (2021), 106664, <https://doi.org/10.1016/j.jcsr.2021.106664>.
- [24] Santa Ana viaduct, Structural health monitoring. <https://cal-sens.com/portfolio/santa-ana-viaduct/> (accessed on October 2022).
- [25] L. Deng, W. Wang, Y. Yu, State-of-The-Art Review on the Causes and Mechanisms of Bridge Collapse, *J. Perform. Constr. Facil.* 30 (2) (2016) 04015005, [https://doi.org/10.1061/\(ASCE\)CF.1943-5509.0000731](https://doi.org/10.1061/(ASCE)CF.1943-5509.0000731).
- [26] A. Ghali, G. Tadros, Bridge progressive collapse vulnerability, *J. Struct. Eng.* 123 (2) (1997) 227–231, [https://doi.org/10.1061/\(ASCE\)0733-9445\(1997\)123:2\(227\)](https://doi.org/10.1061/(ASCE)0733-9445(1997)123:2(227)).
- [27] M. Wang, Z. Zhou, Progressive collapse and structural robustness of bridges, *Appl. Mech. Mater.* 193–194 (2012) 1021–1024, <https://doi.org/10.4028/www.scientific.net/AMM.193-194.1021>.
- [28] H. Jiang, J. Wang, M.G. Chorzepa, J. Zhao, Numerical investigation of progressive collapse of a multispan continuous bridge subjected to vessel collision, *J. Bridge Eng.* 22 (5) (2017) 04017008, [https://doi.org/10.1061/\(ASCE\)BE.1943-5592.0001037](https://doi.org/10.1061/(ASCE)BE.1943-5592.0001037).
- [29] U. Starossek, Avoiding disproportionate collapse of major bridges, *Struct. Eng. Int.* 19 (3) (2009) 289–297, <https://doi.org/10.2749/101686609788957838>.
- [30] F. Bontempi, Elementary concepts of structural robustness of bridges and viaducts, *J. Civ. Struct. Health Monit.* 9 (5) (2019) 703–717, <https://doi.org/10.1007/s13349-019-00362-7>.
- [31] P. Olmati, F. Brando, K. Gkoumas, Robustness assessment of a steel truss bridge, *Structures Congress 2013: Bridging Your Passion with Your Profession* (2013) 250–261. 10.1061/9780784412848.023.
- [32] Leica Geosystems. <https://leica-geosystems.com/> (accessed on May 2022).
- [33] F. Potenza, C. Rinaldi, E. Ottaviano, V. Gattulli, A robotics and computer-aided procedure for defect evaluation in bridge inspection, *J. Civ. Struct. Health Monit.* 10 (3) (2020) 471–484, <https://doi.org/10.1007/s13349-020-00395-3>.
- [34] S. Juárez, A. González, G. Rubio, D. Rodríguez, E. Ottaviano, F.J. Castillo, Closed loop cable robot for large horizontal workspaces, *Smart Struct. Syst.* 27 (2) (2021) 397–406. 10.12989/sss.2021.27.2.397.
- [35] G. Rubio, S. Juárez, A. Gonzalez, D. Rodríguez, L. Corral, A.I. López, I. Payo, F.J. Castillo, New sensor device to accurately measure cable tension in cable-driven parallel robots, *Sensors* 21 (11) (2021) 3604, <https://doi.org/10.3390/s21113604>.
- [36] C. Rinaldi, U. Di Sabatino, F. Potenza, V. Gattulli, Robotized inspection and health monitoring in the Gran Sasso National Laboratory, *Struct. Monit. Maintenance* 8 (1) (2021) 51–67. 10.12989/smm.2021.8.1.051.
- [37] F. Benedettini, C. Gentile, Operational modal testing and FE model tuning of a cable-stayed bridge, *Eng. Struct.* 33 (6) (2011) 2063–2073, <https://doi.org/10.1016/j.engstruct.2011.02.046>.
- [38] B. Peeters, C.E. Ventura, Comparative study of modal analysis techniques for bridge dynamic characteristics, *Mech. Syst. Signal Process.* 17 (5) (2003) 965–988, <https://doi.org/10.1006/mssp.2002.1568>.
- [39] C. Ranieri, G. Fabbrocino, *Operational Modal Analysis of Civil Engineering Structures*, Springer Science + Business Media, New York (2014), <https://doi.org/10.1007/978-1-4939-0767-0>.
- [40] C.A. Brebbia, J.C.F. Telles, L.C. Wrobel, *Boundary Integral Formulation for Inelastic Problems*, *Boundary Element Techniques*, Springer, Berlin (1984), [https://doi.org/10.1007/978-3-642-48860-3\\_6](https://doi.org/10.1007/978-3-642-48860-3_6).
- [41] T. Bratanow, G. De Grande, Numerical analysis of normal stresses in non-Newtonian boundary layer flow, *Engineering Analysis* 2 (1) (1985) 20–25, [https://doi.org/10.1016/0264-682X\(85\)90046-2](https://doi.org/10.1016/0264-682X(85)90046-2).
- [42] Y.C. Ni, M.M. Alamdari, X.W. Ye, F.L. Zhang, Fast operational modal analysis of a single-tower cable-stayed bridge by a Bayesian method, *Meas. J. Int. Meas. Confed.* 174 (2001), 109048, <https://doi.org/10.1016/j.measurement.2021.109048>.
- [43] F. Magalhães, A. Cunha, Explaining operational modal analysis with data from an arch bridge, *Mech. Syst. Signal Process.* 25 (5) (2011) 1431–1450, <https://doi.org/10.1016/j.ymsp.2010.08.001>.
- [44] F. Ubertini, C. Gentile, A.L. Materazzi, Automated modal identification in operational conditions and its application to bridges, *Eng. Struct.* 46 (2013) 264–278, <https://doi.org/10.1016/j.engstruct.2012.07.031>.
- [45] M. He, P. Liang, J. Li, Y. Zhang, Y. Liu, Fully automated precise operational modal identification, *Eng. Struct.* 234 (2021), 111988, <https://doi.org/10.1016/j.engstruct.2021.111988>.
- [46] Y. He, J.P. Yang, X. Li, A three-stage automated modal identification framework for bridge parameters based on frequency uncertainty and density clustering, *Eng. Struct.* 255 (2022), 113891, <https://doi.org/10.1016/j.engstruct.2022.113891>.
- [47] A.K. Pandey, M. Biswas, M.M. Samman, Damage detection from changes in curvature mode shapes, *J. Sound Vib.* 145 (2) (1991) 321–332, [https://doi.org/10.1016/0022-460X\(91\)90595-B](https://doi.org/10.1016/0022-460X(91)90595-B).
- [48] Y. Wang, T.M.S. Elhag, A comparison of neural network, evidential reasoning and multiple regression analysis in modelling bridge risks, *Expert Sys. Appl.* 32 (2) (2007) 336–348, <https://doi.org/10.1016/j.eswa.2005.11.029>.
- [49] N.A.J. Lieven, D.J. Ewins, Spatial correlation of mode shapes: the coordinate modal assurance criterion (COMAC), in: *Proceedings of the 6th International Modal Analysis Conference (IMAC)*, 1988, pp. 690–695.
- [50] J. Kullaa, *Vibration-Based Structural Health Monitoring Under Variable Environmental or Operational Conditions*, in: A. Deraemaeker, K. Worden (Eds.), *New Trends in Vibration Based Structural Health Monitoring*, CISM Courses and Lectures, vol 520, Springer, Vienna (2010). 10.1007/978-3-7091-0399-9\_4.
- [51] R. Gorgin, Y. Luo, Z. Wu, Environmental and operational conditions effects on Lamb wave based structural health monitoring system: A review, *Ultrasonics* 105 (2020), 106114, <https://doi.org/10.1016/j.ultras.2020.106114>.
- [52] B. Peeters, G. De Roeck, One-year monitoring of the Z24-bridge: Environmental effects versus damage events, *Earthq. Eng. Struct. Dyn.* 30 (2) (2001) 149–171, [https://doi.org/10.1002/1096-9845\(200102\)30:2<149::AID-EQE1>3.0.CO;2-Z](https://doi.org/10.1002/1096-9845(200102)30:2<149::AID-EQE1>3.0.CO;2-Z).
- [53] E. Reynders, G. Wursten, G. De Roeck, Output-only structural health monitoring in changing environmental conditions by means of nonlinear system identification, *Struct. Health Monit.* 13 (1) (2014) 82–93, <https://doi.org/10.1177/1475921713502836>.
- [54] K. Maes, L. Van Meerbeek, E.P.B. Reynders, G. Lombaert, Validation of vibration-based structural health monitoring on retrofitted railway bridge KW51, *Mech. Syst. Signal Process.* 165 (2022), 108380, <https://doi.org/10.1016/j.ymsp.2021.108380>.
- [55] R.M. Azzara, G. De Roeck, M. Girardi, C. Padovani, D. Pellegrini, E. Reynders, The influence of environmental parameters on the dynamic behaviour of the San Frediano bell tower in Lucca, *Eng. Struct.* 156 (2018) 175–187, <https://doi.org/10.1016/j.engstruct.2017.10.045>.
- [56] J. Biliszczuk, P. Hawryszków, M. Teichgraber, SHM system and a FEM model-based force analysis assessment in stay cables, *Sensors* 21 (6) (2021) 1927, <https://doi.org/10.3390/s21061927>.
- [57] E. Cheynet, Operational modal analysis with automated SSI-COV algorithm, Zenodo (2020), <https://doi.org/10.5281/ZENODO.3774061>.
- [58] SAP2000 v24, *Structural Analysis and Design*, CSI Analysis Reference Manual, Computers & Structures, INC. (2022).
- [59] M. Levy, M. Salvadori, *Perché gli edifici cadono*, Bompiani ISBN (1997) 8845231070.
- [60] G. Anitori, J.R. Casas, M. Ghosn, Redundancy and Robustness in the Design and Evaluation of Bridges: European and North American Perspectives, *J. Bridge Eng.* 18 (12) (2013) 1241–1251, [https://doi.org/10.1061/\(asce\)be.1943-5592.0000545](https://doi.org/10.1061/(asce)be.1943-5592.0000545).
- [61] M.C. Porcu, D.M. Patteri, S. Melis, F. Aymerich, Effectiveness of the FRF curvature technique for structural health monitoring, *Constr. Build. Mater.* 226 (2019) 173–187, <https://doi.org/10.1016/j.conbuildmat.2019.07.123>.